Theoretical Study of The Electromagnetic Structure of Boron Isotopes Using Local Scale Transformation Technique

Saja H. Mohammed[*], Arkan R. Ridha

Department of Physics, College of Science, University of Baghdad, Baghdad, Iraq

Abstract

The radial wavefunctions of transformed harmonic-oscillator in the local scale transformation technique are used to calculate the root-mean square proton, charge, neutron and matter radii, nuclear density distributions and elastic electron scattering charge form factors of stable (^{10,11}B) and (unstable) exotic (^{8,14,17}B) Boron isotopes. For ^{10}B and ^{11}B, the transformed harmonic-oscillator wavefunctions are applied to all subshells in no-core shell model approach using wbp interaction. For ^{8,14,17}B, the radial wavefunctions of harmonic-oscillator and THO are used to calculate the aforementioned quantities for the core and halo parts, respectively. The calculated matter and charge density distributions are found to be in very good agreement with experimental data for ^{8,14,17}B and ^{10,11}B, respectively. The calculated elastic electron scattering form factors of the longitudinal C0+C2 components for ^{10,11}B are in very good agreement with experimental data.

Keywords: exotic nuclei, nuclear density distributions, elastic electron scattering form factors, proton, charge, neutron and matter *rms* radii.

<div dir="rtl">

دراسة نظرية للتركيب الكهرومغناطيسي لنظائر البورون باستخدام تقنية تحويل المقياس الموضعي

سجى حازم محمد [*]، أركان رفعه رضا

قسم الفيزياء، كلية العلوم، جامعة بغداد، بغداد، العراق

الخلاصة

تم استخدام الدوال الموجية المحولة لجهد المتذبذب التوافقي باستخدام تقنية تحويل المقياس الموضعي لحساب انصاف الاقطار البروتونية والشحنية والنيوترونية والنيوكليونية وتوزيعات الكثافة النووية وعوامل التشكل الشحنية للاستطارة الالكترونية المرنة لنظائر البورون المستقرة (^{10,11}B) وغير المستقرة (^{8,14,17}B). بالنسبة للنواتين ^{10}B و ^{11}B، تم تطبيق الدوال الموجية للمتذبذب التوافقي المحولة على كل القشر الثانوية بنموذج القشرة عديم القلب باستخدام تفاعل واربيرتين-براون. بالنسبة للنوى ^{8,14,17}B، الدوال الموجية القطرية للمتذبذب التوافقي والمتذبذب التوافقي المحولة تم استخدامها لحساب الكميات المذكورة اعلاه لجزئي القلب والهالة، بالتتابع. وجد بان توزيعات الكثافة الكتلية والشحنية المحسوبة هي بتطابق جيد جدا مع تلكم العملية فيما يخص ^{8,14,17}B و ^{10,11}B، بالتتابع. عوامل التشكل المحسوبة للاستطارة الالكترونية المرنة للمركبة الطولية C0+C2 للنوى ^{10,11}B هي بتطابق جيد جدا مع القيم العملية.

</div>

Introduction

The nuclear sizes and density distributions of nuclei are of a great importance in nuclear physics; they are related to the wavefunctions of protons and neutrons [1]. Historically, the charge radius can be found by electron scattering, muonic atoms, K_α X-ray isotope shift and optical isotope shift. Most

---

*Email: Saja.alazawi94@gmail.com

experimental methods use hadron induce reactions such (pions, protons, α or kaon scattering) from nuclei to find the matter radius [2]. The discovery of large reaction cross section(σ_R) of some neutron-rich nuclei, such as ^{11}Li and ^{6}He in comparison with the rest of isotopes of the same element by Tanihata et al. [3] was explained by the existence of long tail in the matter density distribution of ^{11}Li. Such long tail leads to the large rms matter radius. Later on such phenomenon leads to the emergency of halo idiom [4]. In addition, the narrow momentum distribution of ^{9}Li resulting from the fragmentation of ^{11}Li at a beam energy of 790 MeV per nucleon confirmed such large spatial extension of the neutron wavefunction of ^{11}Li by Kobayashi et al.,[5]. Halo nuclei are in general characterized by long tail in density distribution resulting from large spatial extension of the last proton/neutron wavefunction due to their low binding energies (tunneling effect), short lifetime and prefer to be in the states with low orbital quantum numbers. Besides, the Borromean halo nuclei [6], are three-body systems consisting of a compact core and loosely two nucleons where none of the two bodies are found in bound state [7]. The NCSM were failed to reproduce the long tail behavior in the density distributions due to Gaussian fall-off of the wavefunctions [8-11]. To overcome the drawback of the defect of the radial wavefunctions of HO, the two-frequency shell model were applied with limited success [12].

Utilizing the radial wavefunctions of HO and THO, the size radii, density distributions, and elastic electron scattering charge form factors of Boron isotopes (^{8}B, ^{10}B,^{11}B ,^{14}B and ^{17}B) are calculated. The THO wavefunctions are applied to ^{10,11}B for all subshells in the NCSM approach. For ^{8,14,17}B, the core and halo parts are studied separately using the HO and THO wavefunctions, respectively.

Theoretical basis

The radial multipole transition density operator of order J and projection M can be written as [13]

$$\hat{\rho}_{JM,t_z} = \sum_{i=1}^{x} \frac{\delta(r-r_i)}{r_i^2} Y_{JM}(\theta_i, \phi_i) \tag{1}$$

where x denotes the number of neutrons (N) or protons (Z), t_z represent the third component of isospin quantum numbers ($t_z = 1/2$ for protons and $t_z = -1/2$ for neutrons) and Y_{JM} is the spherical harmonics. The nuclear matrix element to Eq. (1) between initial and final nuclear states can be written as [13]

$$\rho_{J,t_z}(r) = \frac{1}{\sqrt{4\pi}} \frac{1}{\sqrt{2J_i+1}} \sum_{ab} X_{b,a,t_z}^{J_f,J_i,J} \langle j_b \| Y_J \| j_a \rangle R_{n_b l_b}(r, b_{t_z}) R_{n_a l_a}(r, b_{t_z}) \tag{2}$$

where J_i and J_f are the total spin of the nucleus in the initial and final states. Besides, a and b denote the single-particle quantum numbers of initial and final states (nlj; n, l and j represent the principal, orbital and total spin quantum numbers of the single nucleon, respectively). $X_{b,a,t_z}^{J_f,J_i,J}$ is the weight of transition calculated from nuclear shell model using *Nushell* code [14] for a given effective interaction and model space. For ground density distribution ($J_f = J_i$, $a = b$ and $J = 0$), Eq. (2) can be reduced to

$$\rho_{J=0,t_z}(r) = \frac{1}{4\pi} \sqrt{\frac{2j_a+1}{2J_i+1}} \sum_a X_{a,a,t_z}^{J_i,J_i,J=0} \left| R_{n_a l_a}(r, b_{t_z}) \right|^2 \tag{3}$$

In the present work, the nuclear density distributions of point neutrons and protons for halo nuclei are calculated using two methods; the first one is by Eq. (3) and the second is by accounting separately the density distribution of two main parts; the core ($\rho_{J=0,t_z}^{core}(r)$) and the halo ($\rho_{J=0,t_z}^{halo}(r)$) as follows [15]

$$\rho_{J=0,t_z}(r) = \rho_{J=0,t_z}^{core}(r) + \rho_{J=0,t_z}^{halo}(r) \tag{4}$$

The core and halo parts are calculated respectively from:

$$\rho_{J=0,t_z}^{core}(r) = \frac{1}{4\pi} \sum_{nl} \xi_{nl,t_z}^{core} \left| R_{nl}(r, b_{t_z}) \right|^2 \tag{5}$$

and

$$\rho_{J=0,t_z}^{halo}(r) = \frac{1}{4\pi} \sum_{nl} \xi_{nl\,t_z}^{halo} \left| R_{nl}(r, b_{t_z}) \right|^2 \tag{6}$$

where ξ_{nl,t_z}^{core} and $\xi_{nl\,t_z}^{halo}$ represent the neutrons or protons occupation number in the nl shells of core and halo respectively. In the present work, ξ_{nl,t_z}^{core} takes integer numbers as predicted by simple shell model. $\rho_{J=0,t_z}^{halo}$ takes assumed fractional real numbers. Due to the Gaussian fall off behaviour of the

radial wavefunction of HO potential. The $R_{nl}(r, b_{t_z})$ in Eqs. (3) and (6) are calculated using the THO radial wavefunctions based on LST as follows [16]:

$$R_{nl}^{THO}(r, b_{t_z}) = \frac{f(r)}{r} \sqrt{\frac{df(r)}{dr}} R_{nl}(f(r), b_{t_z}) \qquad (7)$$

and

$$f(r) = \left[\frac{1}{\left(\frac{1}{r}\right)^m + \left(\frac{1}{\gamma\sqrt{r}}\right)^m}\right]^{\frac{1}{m}} \qquad (8)$$

where $f(r)$ in Eqs. (7) and (8), represent a function chosen so as to reproduce the proper asymptotic condition (exponential shape) for the density distribution at large r, besides it leaves the interior shape of density unchanged [17]. m and γ in Eq. (8) are an integer and real numbers controls how sharply the tail of wavefunction will be. Therefore, Eq. (3) and (4) become, respectively as follows [25]:

$$\rho_{J=0,t_z}(r) = \frac{1}{4\pi} \sqrt{\frac{2j_a+1}{2J_i+1}} \sum_a X_{a,a,t_z}^{J_i, J_i, J=0} |R_{nl}^{THO}(r, b_{t_z})|^2 \qquad (9)$$

and

$$\rho_{J=0,t_z}(r) = \frac{1}{4\pi} \sum_{nl} \xi_{nl,t_z}^{core} |R_{nl}(r, b_{t_z})|^2 + \frac{1}{4\pi} \sum_{nlj} \xi_{nl\,t_z}^{halo} |R_{nl}^{THO}(r, b_{t_z})|^2 \qquad (10)$$

In this work, the two main methods in Eq. (9) and (10) are denoted by LST and HO+LST, respectively. The matter density distributions can be written as:

$$\rho_m(r) = \rho_{J=0,m}^{core}(r) + \rho_{J=0,m}^{halo}(r) \qquad (11)$$

where

$$\rho_m^{core}(r) = \rho_{J=0,t_z=1/2}^{core}(r) + \rho_{J=0,t_z=-1/2}^{core}(r) \qquad (12)$$

and

$$\rho_{J=0,m}^{halo}(r) = \rho_{J=0,t_z=+/-1/2}^{halo}(r) \qquad (13)$$

The total charge density distribution $\rho_{ch}(r)$ (CDD) coming from protons and neutrons can be written as

$$\rho_{ch}(r) = \rho_{ch,t_z=1/2}(r) + \rho_{ch,t_z=-1/2}(r) \qquad (14)$$

The first and second terms in Eq. (14) are obtained by taking the folding of single proton/neutron charge density (ρ_{pr}/ρ_{neu}) into the distribution of the point proton/neutron density in Eqs. (9) or (10) as follows:

$$\rho_{ch,t_z=1/2}(r) = \int \rho_{J=0,t_z=1/2}(r)\rho_{pr}(\mathbf{r} - \mathbf{r}')d\mathbf{r}' \qquad (15)$$

and

$$\rho_{ch,t_z=-1/2}(r) = \int \rho_{J=0,t_z=-1/2}(r)\rho_{neu}(\mathbf{r} - \mathbf{r}')d\mathbf{r}' \qquad (16)$$

where $\rho_{pr}(\vec{r})$ [18] and $\rho_{neu}(\vec{r})$ [19] takes, respectively the following forms:

$$\rho_{pr}(r) = \frac{1}{(\sqrt{\pi}a_{pr})^3} e^{\left(\frac{-r^2}{a_{pr}^2}\right)} \qquad (17)$$

and

$$\rho_{neu}(r) = \frac{1}{(\pi r_i^2)^{3/2}} \sum_1^2 \theta_i\, e^{-r^2/r_i^2} \qquad (18)$$

In Eq. (17), $a_{pr} = 0.65\, fm$ such value reproduces the experimental charge rms radius of the proton ($\langle r^2 \rangle_{pr}^{1/2} = \left(\frac{3}{2}\right)^{1/2} a_{pr} \approx 0.8\, fm$). In Eq. (18), the parameter θ_i and r_i are given in Table-1.

Table 1-Parameters of the neutron charge distributions.

θ_1	1
θ_2	-1
r_1^2 (fm^2)	0.469
r_2^2 (fm^2)	0.546

The rms radii of neutron, proton and matter are calculated from [20]

$$\langle r^2 \rangle_X^{1/2} = \sqrt{\frac{4\pi}{X} \int_0^\infty \rho_{J=0,X}(r) r^2 dr} \tag{19}$$

where X stands for N (number of neutrons), Z (atomic number), and A (mass number), respectively. The rms charge radii are calculated from

$$\langle r^2 \rangle_{ch}^{1/2} = \sqrt{\frac{4\pi}{Z} \int_0^\infty \rho_{J=0,ch}(r) r^2 dr} \tag{20}$$

Finally, the longitudinal electron scattering form factors in the first Born approximation can be written as [21,22]:

$$F_{J,ch}^C(q) = \frac{1}{Z} \sqrt{\frac{4\pi}{(2J_i+1)}} \sum_{t_z} \langle J_f \| \boldsymbol{O}_J^C(q,t_z) \| J_i \rangle f_{t_z}(q) \tag{21}$$

or in more compact form as

$$F_{J,ch}^C(q) = \sum_{t_z} F_J^C(q,t_z) f_{t_z}(q) \tag{22}$$

where

$$F_J^C(q,t_z) = \frac{1}{Z} \sqrt{\frac{4\pi}{(2J_i+1)}} \langle J_f \| \boldsymbol{O}_J^C(q,t_z) \| J_i \rangle \tag{23}$$

In Eqs. (21-23), q represents the momentum transfer from electrons to the nucleus. $|J_i\rangle$ and $|J_f\rangle$ are initial and final states of the nucleus. $f_{t_z}(q)$ is the charge form factor of a single proton and neutron given by taking Fourier transforms to Eqs. (17) and (18), respectively. $\boldsymbol{O}_{J,t_z=1/2}^C(q)$ represents the Coulomb multipole operator of the longitudinal electron scattering given by [23]:

$$\boldsymbol{O}_{JM_J}^C(q,t_z) = \int j_J(qr) Y_{JM_J}(\Omega_r) \hat{\rho}_{t_z}(\vec{r}) \tag{24}$$

where $\hat{\rho}_{t_z}(\vec{r})$ represents the density operator given in ref. [21]. The reduced matrix element in Eqs. (21) and (23) can be written in terms of the reduced matrix element of a single nucleon matrix element as [22]

$$\langle J_f \| \boldsymbol{O}_J^C(q,t_z) \| J_i \rangle = \sum_{ab} X_{a,b,p/n}^{J_i,J_f,J} \langle b,t_z \| O_J^C(q,r,t_z) \| a,t_z \rangle \tag{25}$$

where

$$O_J^C(q,r,t_z) = e_{t_z} j_J(qr) Y_J(\Omega_r) \tag{26}$$

The single nucleon matrix element in Eq. (25) is given by [23]

$$\langle b,t_z \| O_J^C(q,r,t_z) \| a,t_z \rangle = e_{t_z} \langle n_b l_b | j_J(qr) | n_a l_a \rangle \langle (l_b 1/2) j_b \| Y_J(\Omega_r) \| (l_a 1/2) j_a \rangle \tag{27}$$

Eq. (21) can be written in terms of transition density distribution as [22]

$$\left| F_{J,ch}^C(q) \right| = \frac{1}{Z} \sqrt{\frac{4\pi}{(2J_i+1)}} \left| \int_0^\infty j_J(qr) \rho_{J,ch}(r) r^2 dr \right| \tag{28}$$

where $j_J(qr)$ and $\rho_{ch,J}(r)$ are spherical Bessel function and charge transition density distribution, respectively. The total longitudinal form factors are given by:

$$|F(q)|^2 = \sum_J \left| F_{J,ch}^C(q) \right|^2 \tag{29}$$

At photon point ($q = w = \frac{E_x}{\hbar c}$), E_x is the excitation energy, Eq. (28) can be written as [22]:

$$\left| F_{J,ch}^C(q=w) \right| = \frac{1}{Z} \sqrt{\frac{4\pi}{(2J_i+1)}} \left(\frac{q^J}{(2J+1)!!} \right) \left| \int_0^\infty \rho_{ch,J}(r) r^{J+2} dr \right| \tag{30}$$

since,

$$\left| \langle J_f \| \boldsymbol{O}_J(\vec{r}) \| J_i \rangle \right| = \left| \int_0^\infty \rho_{J,ch}(r) r^{J+2} dr \right| \tag{31}$$

Therefore, Eq. (28) can be written as:

$$\left| F_{J,ch}^C(q=w) \right| = \frac{1}{Z} \sqrt{\frac{4\pi}{(2J_i+1)}} \left(\frac{q^J}{(2J+1)!!} \right) \left| \langle J_f \| \boldsymbol{O}_J(\vec{r}) \| J_i \rangle \right| \tag{32}$$

From Eq. (32), the multiparticle reduced matrix element of electric multipole operator can be written as [22]:

$$\langle J_f \| \boldsymbol{O}_J(\vec{r}) \| J_i \rangle = Z \frac{(2J+1)!!}{q^J} \sqrt{\frac{(2J_i+1)}{4\pi}} F_{J,ch}^C(q=w) \tag{33}$$

The quadrupole moment is related to the multiparticle reduced matrix element of electric multipole operator by the relation [24]

$$Q = \sqrt{\frac{16\pi}{5}} \begin{pmatrix} J & 2 & J \\ -J & 0 & J \end{pmatrix} \langle J_f \| \boldsymbol{O}_J (\vec{r}) \| J_i \rangle \tag{34}$$

Therefore, the quadrupole moment can be reduced to the following final formula:

$$Q = \sqrt{\frac{16\pi}{5}} \begin{pmatrix} J & 2 & J \\ -J & 0 & J \end{pmatrix} \frac{(2J+1)!!Z}{q^J} \sqrt{\frac{(2J_i+1)}{4\pi}} F^C_{J=2,ch}(q = w) \tag{35}$$

The transition density distribution in Eq. (28) is coming from contribution of core-polarization (CP) and model-space (MS) as follows [25]

$$\rho_{J,ch}(r) = \rho^{CP}_{J,ch}(r) + \rho^{MS}_{J,ch}(r) \tag{36}$$

In the work, $\rho^{CP}_{ch,J}(r)$ is calculated using Tassie [26] and Bohr-Mottelson [27] models, respectively as:

$$\rho_{ch,J}(r) = N r^{J-1} \frac{d}{dr} \rho_{ch}(r) \tag{37}$$

and

$$\rho_{ch,J}(r) = N \frac{d}{dr} \rho_{ch}(r) \tag{38}$$

where N in Eqs. (37) and (38) represents the normalization constant is fixed so as to reproduce the experimental quadrupole moment.

Results and Discussion

The LST which is a correction to the radial wavefunctions of HO potential is applied to calculate the ground state properties of Boron isotopes which is suitable to regenerate the long tail feature of the density distribution in order to get rid of the steep slope or Gaussian fall off behaviour of HO wavefunctions.

The ground properties of the Boron isotopes (^{8,10,11,14,17}B); J^π, half-life time, type of nuclear sample (whether proton or neutron rich nuclei) and separation energies are presented in Table-2.

The parameters of HO and THO needed to fulfill the calculations of the nuclei under study; HO size parameters (b_p and b_n), occupation numbers, m, and γ are presented in Table-3. These parameters are adopted so as to reproduce the experimental rms radii for the isotopes under study.

The calculated proton, charge, neutron, and matter rms radii for boron isotopes (^{8,14,17}B) using HO+LST technique compared with available experimental data are shown in Table-4.

The HO size parameters (b_p and b_n), m and $\gamma_{p,n}$ for NCSM calculations of (^{8,10,11}B) are presented in Table 5. The same things that in Table 4, but using the NCSM technique of (^{8,10,11}B) in Table-6. Very good agreements are obtained for the calculated rms radii in comparison with the experimental data for all isotopes under study in HO+LST technique.

In Table-7, the calculated proton, charge, neutron, and matter rms radii for ^{8,10,11,14,17}B using HO technique are compared with available experimental data.

The calculated MDDs for ^{8}B, ^{14}B and ^{17}B are presented in Figures-1(a, b, c), respectively. In Fig. 1(a) for ^{8}B, the black solid, red solid and blue dashed curves represent the calculated MDDs using HO+LST, LST and HO, respectively. It is clear that the result of HO+LST is in good agreement with experimental data for all r regions. The result of LST is underestimated the tail region. In Fig. 1(b), for ^{14}B, the black solid and blue dashed curves represent the calculated MDDs using HO+LST and HO, respectively. It is apparent that there is a good agreement in comparison with experimental in HO+LST. Finally, in Figure-1(c), the black solid, short red dashed and long blue dashed are the calculated MDDS using HO+LST(sdpfnow [28]), HO+LST(assumed ξ) and HO, respectively. In the HO+LST(assumed ξ), the filling numbers for two neutron halo are predicted to be in subshells, $1d_{5/2}$, $1d_{3/2}$, $2S_{1/2}$, $1f_{7/2}$, $2P_{3/2}$ and $2P_{1/2}$. It is apparent that there is a good agreement in comparison with experimental in HO+LST(assumed ξ). It is clear in Figures 1-(a, b, c), that the results of HO is completely failed to regenerate the long tail behaviour.

The calculated neutron and proton density distributions in HO+LST(assumed ξ) for ^{8}B,^{14}B and ^{17}B are depicted in Figures 2-(a, b, c), respectively. It is obvious that the long tail characteristic is well produced in the proton density distribution for ^{8}B, besides in the neutron density distribution for ^{14,17}B and this is attributed to the parameters used in Table-2 which leads to such well produced long tail in LST.

The charge density distributions of stable ^{10,11}B are portrayed in Figure-3(a, b), respectively. In both isotopes, the NCSM approach are applied using warburton-brown interaction [29] and *spsdpf* model space with THO wavefunctions.

The calculated charge form factors of the component C0+C2 for ^{10,11}B are shown in Figure- 4(a, b), respectively. The solid and dashed curves in both isotopes represent the calculated charge form factor using Tassie and Bohr-Mottelson models, respectively. It is obvious for both figures that the results of Bohr-Mottelson model are in good agreement with experimental data.

In Figures-5 (a, b), the charge form factors of the component C0 are calculated for even (^{8,10,14}B) and odd (^{11,17}B) boron isotopes, respectively. It is clear from both figures that the increase in neutron numbers lead the calculated form factors to be shifted downwards and backwards, reducing the charge form factors due the screening effect of neutron excess.

Table 2- Properties of boron isotopes (^{8}B,^{10}B,^{11}B,^{14}B and ^{17}B).

$^{A}_{Z}X_{N}$	J^{π}[30]	Half-Life Time [30]	Type [31]	Separation Energies in MeV [32]
$^{8}_{5}B_{3}$	2^{+}	$t_{1/2} = 770\ ms$	^{7}Be+One proton halo	$S_p = 0.136$
$^{10}_{5}B_{5}$	3^{+}	Stable	Stable	$S_p = 6.586$ $S_n = 8.437$
$^{11}_{5}B_{6}$	$(3/2)^{-}$	Stable	Stable	$S_p = 11.228$ $S_n = 11.454$
$^{14}_{5}B_{9}$	2^{-}	$t_{1/2} = 13.8\ ms$	^{13}B+One neutron halo	$S_n = 0.970$
$^{17}_{5}B_{12}$	$(3/2)^{-}$	$t_{1/2} = 5.08\ ms$	^{15}B+Two neutrons halo	$S_{2n} = 1.38$

Table 3-The HO size parameters and $\gamma_{p,n}$ of ^{8}B ,^{14}B and ^{17}B using HO+LST calculations.

$^{A}_{Z}X_{N}$	$b_p(fm)$	$b_n(fm)$	nl_j	Occupation number	m	γ_p (fm^{-1})	γ_n (fm^{-1})
$^{8}_{5}B_{3}$	1.575	1.54	1P$_{1/2}$	0.98	18	1.293	1.309
			2S$_{1/2}$	0.01			
			2p$_{3/2}$	0.01			
$^{14}_{5}B_{9}$	1.698	1.8	1d$_{5/2}$	0.5	12	1.453	1.528
			1d$_{3/2}$	0.2			
			2S$_{1/2}$	0.3			
$^{17}_{5}B_{12}$	1.815	1.869	1d$_{5/2}$	0.5	20	2.504	1.868
			1d$_{3/2}$	0.45			
			2S$_{1/2}$	0.9			
			1f$_{7/2}$	0.05			
			2P$_{3/2}$	0.05			
			2P$_{1/2}$	0.05			

Table 4-Calculated proton, charge, neutron, and matter rms radii in Fermi's for boron isotopes ^{8}B,^{14}B and ^{17}B by using HO+LST technique compared with available experimental data.

$^A_Z X_N$	$\langle r^2\rangle_p^{1/2}$	Exp. $\langle r^2\rangle_p^{1/2}$	$\langle r^2\rangle_{ch}^{1/2}$	Exp. $\langle r^2\rangle_{ch}^{1/2}$	$\langle r^2\rangle_n^{1/2}$	Exp. $\langle r^2\rangle_n^{1/2}$	$\langle r^2\rangle_m^{1/2}$	Exp. $\langle r^2\rangle_m^{1/2}$
$^8_5 B_3$	2.823	2.76(8) [33]	2.866	2.82(6) [34]	2.085	2.16(8) [33]	2.571	2.55(8) [33]
$^{14}_5 B_9$	2.460	2.46(7) [37]	2.547	___	3.173	___	2.938	3.00(10) [36]
$^{17}_5 B_{12}$	2.63	2.63(7) [37]	2.697	___	3.237	___	3.072	3.00(6) [38]

Table 5-The HO size parameters, m and $\gamma_{p,n}$ for NCSM calculations of ^{8}B ,^{10}B and ^{11}B.

$^A_Z X_N$	$b_p(fm)$	$b_n(fm)$	nl_j	m	γ_p (fm^{-1})	γ_n (fm^{-1})
$^8_5 B_3$	1.656	1.523	*spsdpf*	20	1.654	2.064
$^{10}_5 B_5$	1.608	1.63	*spsdpf*	24	2.428	2.462
$^{11}_5 B_6$	1.588	1.83	*spsdpf*	20	2.297	2.648

Table 6-Calculated proton, charge, neutron, and matter rms radii in Fermi's of (^{8}B,^{10}B and ^{11}B)

$^A_Z X_N$	b_p (fm)	b_n (fm)	$\langle r^2\rangle_p^{1/2}$	Exp. $\langle r^2\rangle_p^{1/2}$	$\langle r^2\rangle_{ch}^{1/2}$	Exp. $\langle r^2\rangle_{ch}^{1/2}$	$\langle r^2\rangle_n^{1/2}$	Exp. $\langle r^2\rangle_n^{1/2}$	$\langle r^2\rangle_m^{1/2}$	Exp. $\langle r^2\rangle_m^{1/2}$
$^8_5 B_3$	1.656	1.523	2.823	2.76(8) [33]	2.920	2.82(6) [34]	2.085	2.16(8) [33]	2.571	2.55(8) [33]
$^{10}_5 B_5$	1.608	1.63	2.342	___	2.45	2.45(12) [35]	2.374	___	2.358	2.56(23) [36]
$^{11}_5 B_6$	1.588	1.83	2.315	___	2.419	2.42(12) [35]	2.707	___	2.536	2.605(9) [36]

by using NCSM calculations compared with available experimental data.

Table 7-Calculated and experimental proton, charge, neutron, and matter rms radii in Fermi's for Boron isotopes (^{8}B, ^{14}B and ^{17}B) using HO technique compared with available experimental data.

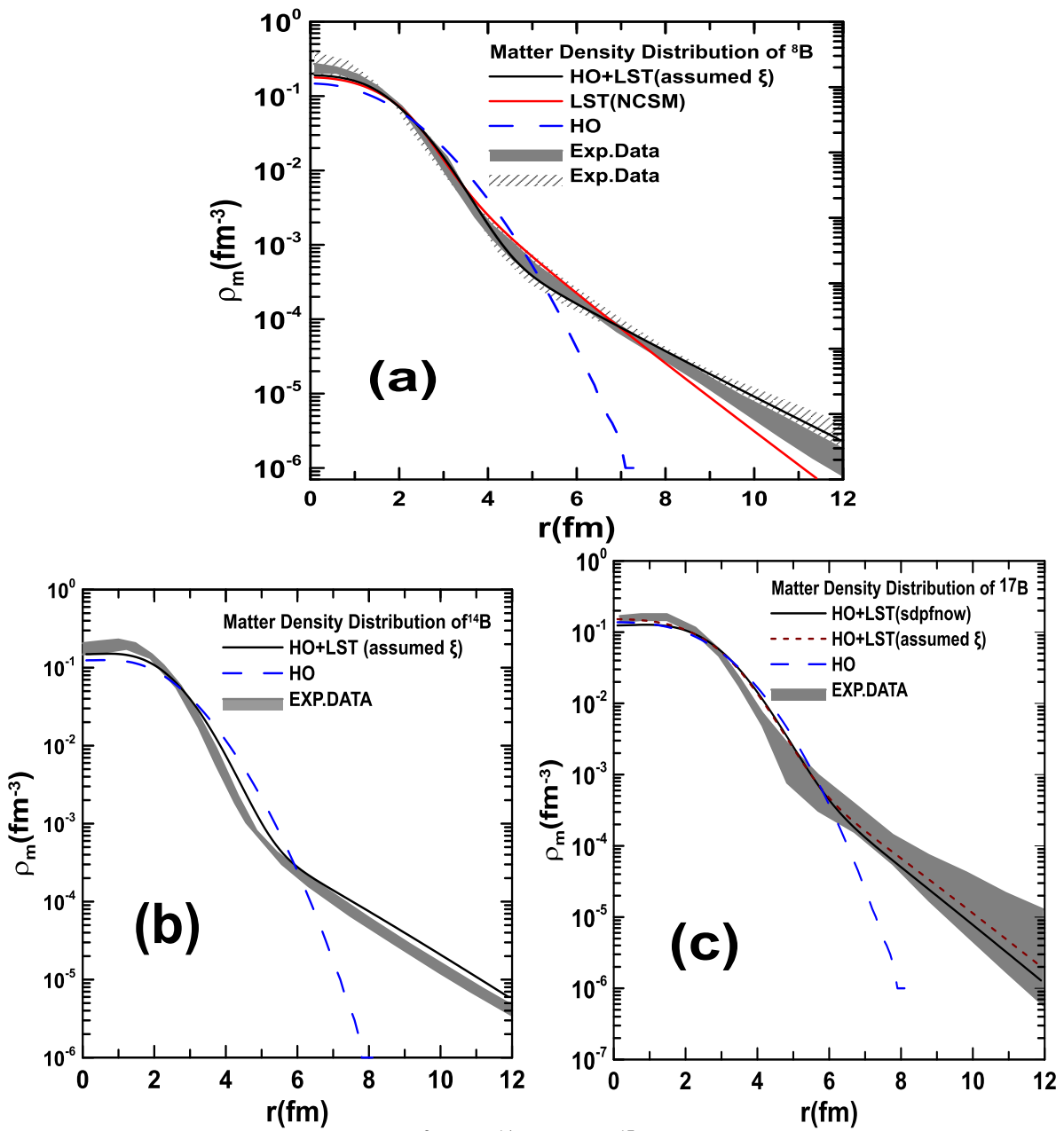| $^A_Z X_N$	b_p (fm)	b_n (fm)	$\langle r^2\rangle_p^{1/2}$	Exp. $\langle r^2\rangle_p^{1/2}$	$\langle r^2\rangle_{ch}^{1/2}$	Exp. $\langle r^2\rangle_{ch}^{1/2}$	$\langle r^2\rangle_n^{1/2}$	Exp. $\langle r^2\rangle_n^{1/2}$	$\langle r^2\rangle_m^{1/2}$	Exp. $\langle r^2\rangle_m^{1/2}$
$^8_5 B_3$	1.945	1.54	2.823	2.76(8) [33]	2.932	2.82(6) [34]	2.085	2.16(8) [33]	2.571	2.55(8) [33]
$^{14}_5 B_9$	1.698	2.053	2.461	2.46(7) [37]	2.545	___	3.173	___	2.938	3.00(10) [33]
$^{17}_5 B_{12}$	1.814	1.978	2.629	2.63(7) [37]	2.695	___	3.238	___	3.071	3.00(6) [38]

Figure 1-Matter density distributions of [8]B (a), [14]B (b) and [17]B (c). The experimental data represented by shaded and hatched area are taken from [39] for [8]B, [40] for [14]B and [41] for [17]B.
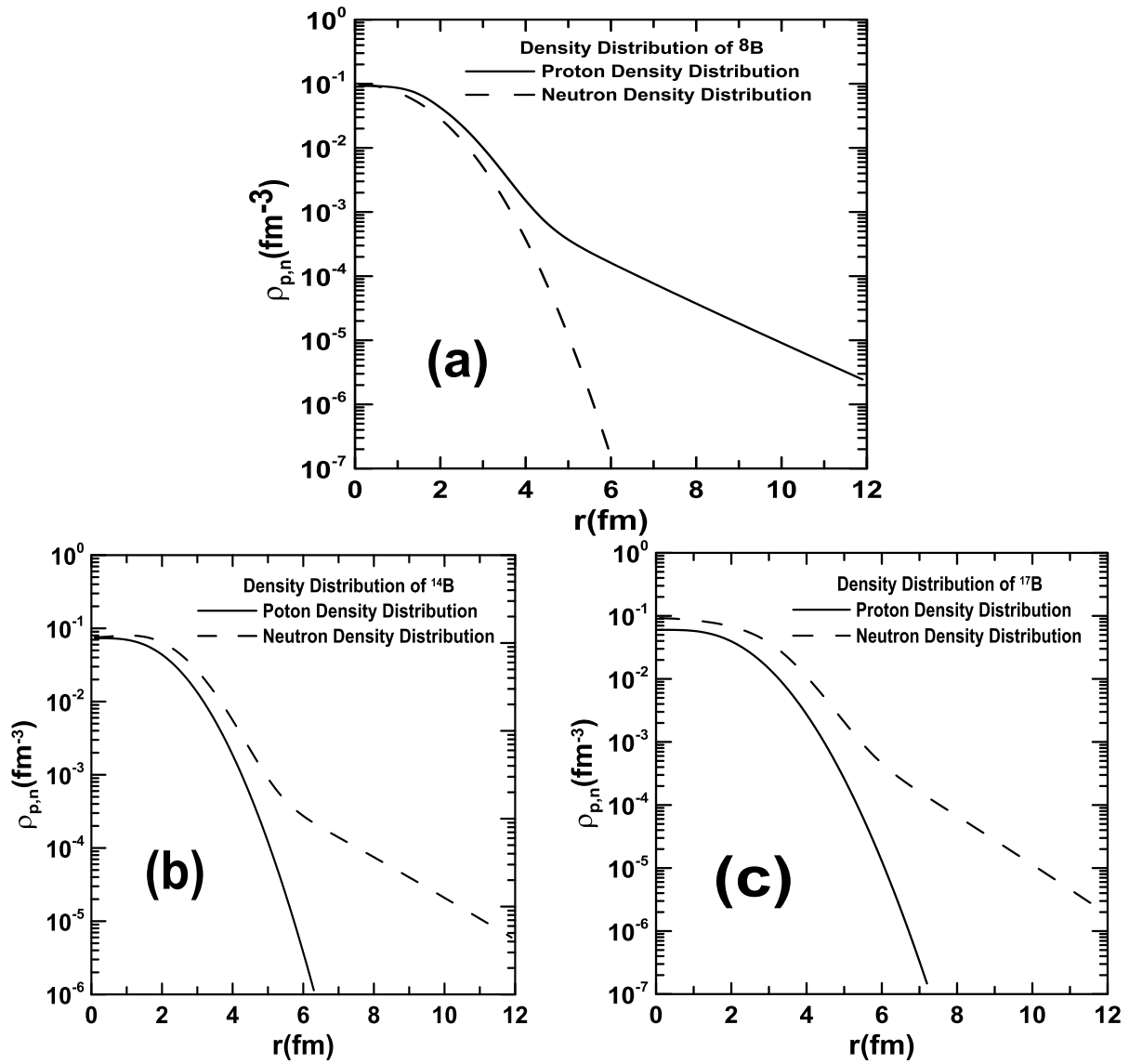
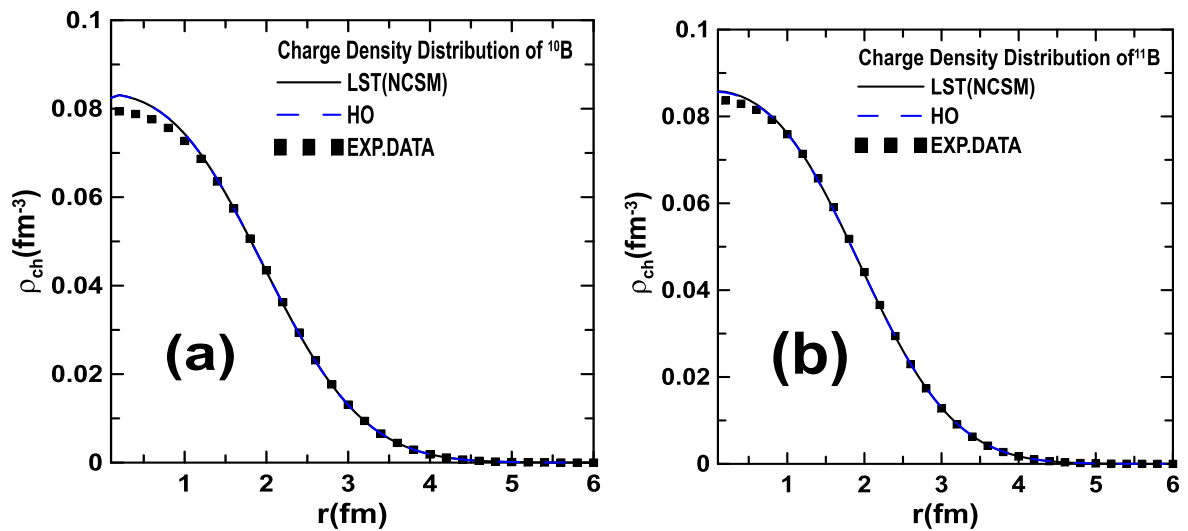**Figure 2-**The neutron and proton density distributions in HO+LST(assumed ξ) for Boron isotopes ^{8}B(a),^{14}B(b),^{17}B(c).

Figure 3-charge density distributions of (a) ^{10}B and (b) ^{11}B. The solid and dashed curves are the results of LST and HO calculations, respectively. The dotted curve in both figures represent experimental data [35].
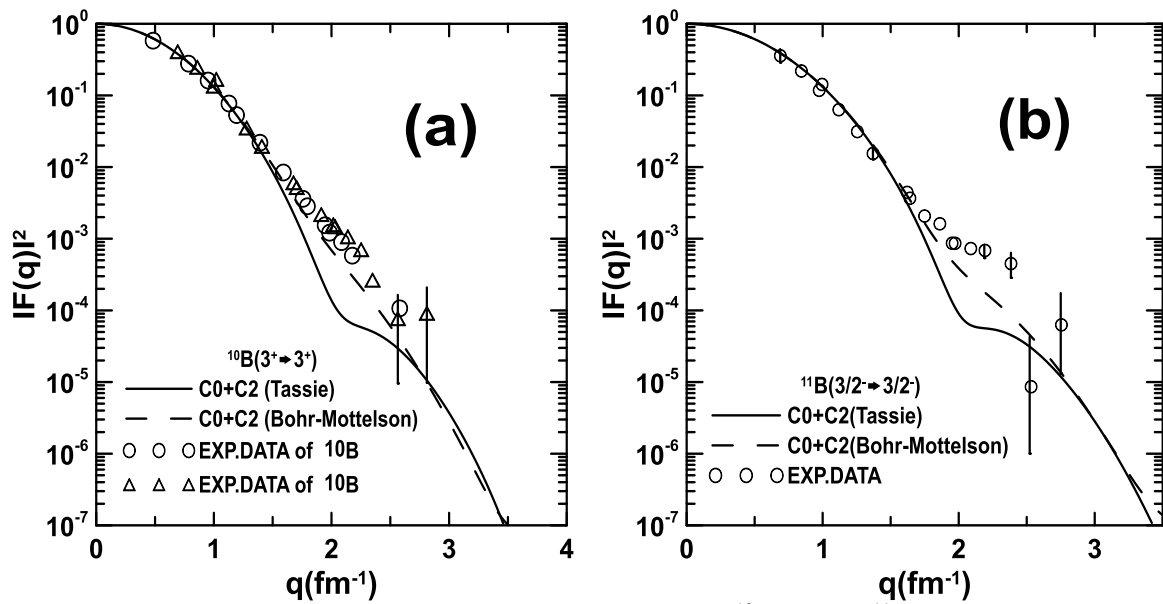
Figure 4-Elastic Coulomb charge form factors (C0+C2) of (a) ^{10}B and (b) ^{11}B. The experimental data for ^{10}B are represented by empty circles [42] and triangles [43]. The experimental data of ^{11}B are represented empty circles [43].
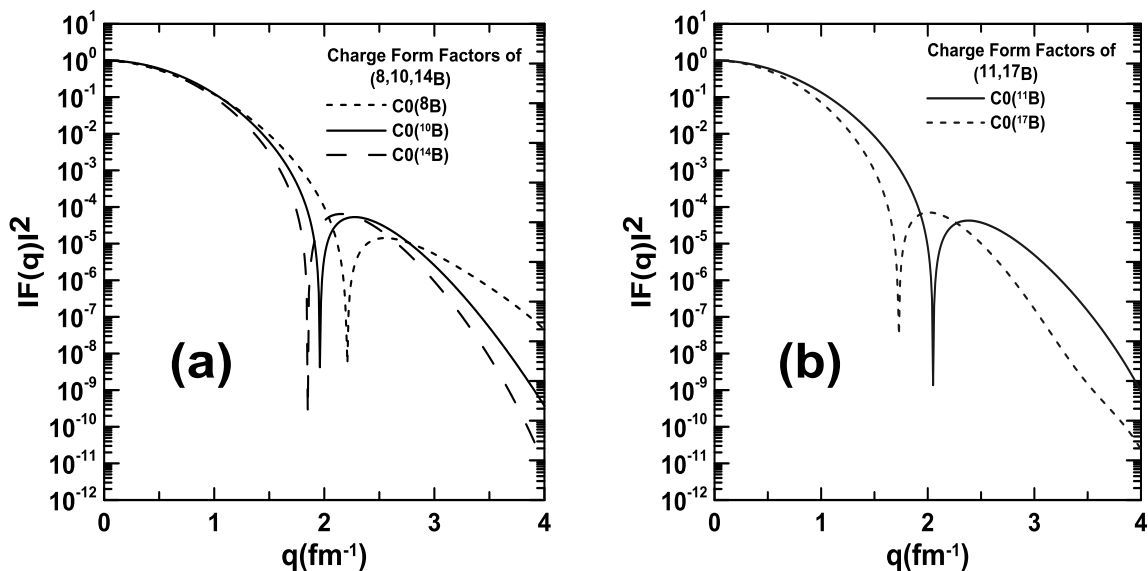

Figure 5-Charge form factors of ^{8,10,14}B(a) and ^{11,17}B (b).

Conclusions

   The transformed harmonic-oscillator (THO) wavefunctions in local scale transformation (LST) technique is used to study the root-mean square (rms) proton, charge, neutron and matter radii, density distributions and elastic electron scattering form factors of Boron isotopes (^{8,10,11,14,17}B). Good agreements are obtained for the calculated rms radii in comparison with experimental data. The long tail behavior which is a main feature of exotic nuclei are well produced by using such modified wavefunctions. Besides, the elastic longitudinal electron scattering form factors of the C0 and C0+C2 components are calculated of exotic (^{8}B,^{14}B and ^{17}B) and stable (^{10}B and ^{11}B) isotopes, respectively. The C2 component are calculated using the Bohr-Mottelson and Tassie models. The results of ^{10}B and ^{11}B are relatively in good agreement with experimental data in Bohr-Mottelson model. The results of exotic isotopes are left for electron-radioactive ion beam colliders where the effect of the excess of protons and neutrons are going to be studied on the charge form factors. Finally, in the present work,

the LST technique is proved itself to be a good technique to study the bulk properties of both stable and exotic nuclei.

References
1. Negele, J.W. **1989**. *Advances in Nuclear Physics*.1st Ed. Springer US, **19**, 1.
2. Donnelly T. W. and Walecka J. D. **1975**. Electron scattering and nuclear structure. *Annu. Rev. Nucl. Sci*. **25**: 329-405.
3. Tanihata, I., Hamagaki H., Hashimoto O., Nagamiya S., Shida Y., Yoshikawa N., Yamakawa O., Sugimoto K., Kobayashi T., Greiner D. E., Takahashi N. and Nojiri Y. **1985.** Measurement of interaction cross sections and radii of He isotopes. *Physics Letters B*, **160**(6): 380-384.
4. Hansen P. G. and Jonson B. **1987**. The neutron halo of extremely neutron-rich nuclei. *Europhysics Letters*, **4**(4): 409-414.
5. Kobayashi T., Yamakawa O., Omata K., Sugimoto K., Shimoda T., Takahashi N and Tanihata I. **1988.** Projectile fragmentation of the extremely neutron-rich nucleus ^{11}Li at 0.79 GeV/nucleon. *Phys.Rev.Lett*., **60**: 2599.
6. Yamasita M. T., de Carvalho R. S. M., Frederico T., and Tomio L. **2009.** Constraints on two-neutron separation energy in the Borromean ^{22}C nucleus. *Phys.Lett., B*, **697**: 90.
7. Zukov M. V., Danilin B. V., Fedorov D. V., Bang J. M., Thompson I. J. and Vaagen J. S. **1993**. Bound state properties of Borromean halo nuclei: P^6He and $P^{11}P$Li. *Physics Reports*. **231**(4): 151-199.
8. Navratil P. and Barrett B. R. **1996.** No-core shell-model calculations with starting-energy-Ndependent multivalued effective interactions. *Physical Review C*. **54**(6): 2986-2995.
9. Navratil P. and Barrett B. R. **1998**. Large-basis shell-model calculations for p-shell nuclei. *Physical Review C*. **57**(6): 3119-3128.
10. Caurier E. and Navratil P. **2006**. Proton radii of ^{4,6,8}He isotopes from high-precision nucleon-nucleon interactions. *Physical Review C*. **73** (021302(R)): 1-5.
11. Hamoudi A. K., Radhi R. A and Ridha A. R. **2015**. Elastic electron scattering from ^{17}Ne and ^{27}P exotic nuclei Nucleus. *Iraqi Journal of Physics*, 13, **28**: 68-81 and R. A. Radhi, A. K. Hamoudi and A. Rifat, Elastic Electron Scattering From Unstable Neutron-Rich ^{19}C Exotic. *Iraqi Journal of Science*. **54** : 324-332.
12. Heyde K. L. G. **1994.** *The Nuclear Shell Model*. Springer Berlin Heidelberg.
13. Satchler G. R. **1983.** *Direct Nuclear Reactions*. Oxford University Press.
14. Brown B. A. and Rae W. D. M**, 2007.** MSU-NSCL report.
15. Hamoudi A. K., Radhi R. A. and Ridha A. R. **2012.** Theoretical study of matter density distribution and elastic electron scattering form factors for the neutron-rich ^{22}C exotic nucleus. *Iraqi Journal of Physics*. 10, **19**: 25-34.
16. Karataglidis, S. and Amos, K. **2005**. Local scale transformations and extended matter distributions in nuclei. *Phys. Rev. C*, **71** (064601): 1-13.
17. Donnelly T. W, Dubach J and Ingo Sick Isospin dependences in parity-violating electron scattering *. Nucl. Phys. A*, **503:** 589.
18. Elton L. R. B. **1961.** "*Nuclear Sizes*", Oxford University Press.
19. Chandra, H. And Sauer, G. **1976.** Relativistic corrections to the elastic electron scattering from ^{208}Pb. *Phys. Rev. C*, **13**: 245-252.
20. Trzcińska A, Jastrzębski J., Lubiński P., Hartmann F. J., Schmidt R., von Egidy T., and Kłos B. **2001**. Neutron Density Distributions Deduced from Antiprotonic Atoms. *Phys. Rev. Lett*. **87**, 082501
21. Deforest T., Jr. and Walecka J. D. **1966.** Electron scattering and nuclear structure. *Advances in Physics*, **15** (57): 1-109.
22. Brown B. A., B. H. Wildenthal, C. F. Williamson, F. N. Rad, S. Kowisiki, H. crannell and J. T. O' Brien. **1985**. Phys. Rev. **C 32**: 1127-1145.
23. Deforest T. Jr. and Walecka, J. D. **1966**. Electron scattering and nuclear structure. *Advances in Physics*, 15: 1-109.
24. Peter Ring and Peter Schuck, **1981.** "*The Nuclear Many-Body Problem*", Springer-Verlag.
25. Brussard P. J. and Glaudemans P. W. M. **1977.** "*Shell-Model Application in Nuclear spectroscopy*", North-Holland, Amesterdam.

26. Bertsch, G. and Tsai S. F. **1974.** How good is the collective model. *Phys. Lett. B*. **50**: 319-322.

27. Bohr A, and Mottelson B. R. **1998.** "*Nuclear Structure Vol II*", World Scientific (**1998**).

28. Nummela S et al. **2001.** Phys. Rev. C **63**: 044316-1.

29. Warburton E. K. and B. A. Brown. **1992.** Effective interactions for the $0p1s0d$ nuclear shell-model space. *Phys. Rev*. C**46**: 923.

30. Audi G., Kondev, F.G., Meng Wang, Huang, W.J. and Naimi, S. **2017**. The NUBASE2016 evaluation of nuclear properties. *Chinese Physics C,* **41** (030001): 1-138.

31. Tanihata, I., Savajols, H. and Kanungo, R. **2013**. Recent experimental progress in nuclear halo structure studies. *Progress in Particle and Nuclear Physics*, **68**: 215-313.

32. Jensen, A. S., Riisager, K. and Fedorov, D. V. **2004**. Structure and reactions of quantum halos . *Reviews of Modern Physics*, **76**: 215-261.

33. Chandel, S. S., Dhiman, S. K. and Shyam, R. **2003.** "Structure of ^{8}B and astrophysical S17 factor in Skyrme Hartree-Fock theory Phys". *Rev. C*, 68: 054320

34. Bertulani C.A. **2007.** Nuclear Physics in a Nutshell. *J. Phys. G* , (34): 315-334   .

35. De Vries H., De Jager C. W and De Vries C. **1987.** (Nuclear charge density distribution parameters from elastic electron scattering). *Atomic Data and Nuclear Data Tables*, **36**: 495.

36. Ozawa A., Suzuki T., and Tanihata I. **2001**. Nuclear size and related topics. *Nuclear Physics A*, 693: 32-62.

37. Estradé A., Kanungo R., Horiuchi W., Ameil F., Atkinson J., Ayyad Y., Cortina-Gil D., Dillmann I., Evdokimov A., Farinon F., Geissel H., Guastalla G., Janik R., Kimura M., Knöbel R., Kurcewicz J., Litvinov Yu. A., Marta M., Mostazo M., Mukha I., Nociforo C., Ong H. J., Pietri S., Prochazka A., Scheidenberger C., Sitar B., Strmen P., Suzuki Y., Takechi M., Tanaka J., Tanihata I., Terashima S.,Vargas J., Weick H and Winfield J. S. Phys. Rev. Lett. Proton Radii of $^{12-17}$B Define a Thick Neutron Surface in ^{17}B, PRL **113**, 132501 (**2014**)

38. Ozawa A., Kobayashi T., Sato H., Hirata D., Tanihata I., Yamakawa O., Interaction cross sections and matter radii of A= 20 isobars. *Phys. Lett. B*. 334: 18.

39. Takechi M., Fukuda M., Mihara, et al. **2005**. *Eur. Phys. J. A*, **25** :217-219.

40. Fukuda1 M., Nishimura D., Suzuki S., Tanaka M., Takechi M., Iwamoto1 K., Wakabayashi S.,Yaguchi M., Ohno J., Morita Y., Kamisho Y., Mihara M., Matsuta K., Nagashima M., Ohtsubo T., Izumikawa T., Ogura T., Abe K., Kikukawa N., Sakai T., Sera D., Suzuki T., Yamaguchi T., Sato K., Furuki H., Miyazawa S., Ichihashi N., Kohno J., Yamaki S., Kitagawa A., Sato S., and Fukuda S. Neutron halo in ^{14}B studied via reaction cross sections, epjconf **66**, 02037, **2014**

41. Yamaguchi Y., Wu C., Suzuki T., Ozawa A., Fang D. Q., Fukuda M., Iwasa N., Izumikawa T., Jeppesen H., Kanungo R., Koyama R., Ohnishi T., Ohtsubo T., Shinozaki W., Suda T., Takahashi M, and Tanihata1 I. **2004.** Density distribution of ^{17}B from a reaction cross-section Measurement. *Phys. Rev. C***, 70**: 054320.

42. Cichocki, A., Dubach, J., Hicks, R. S., Peterson, G. A., De Jager, C. W., De Vries, H., Kalantar-Nayestanaki, N. and Sato, T. **1995**. Electron scattering from ^{10}B. *Physical Review C*, **51**: 2406-2426.

43. Stovall, T., Goldemberg, J. and Isabelle, D. B. **1966**. Coulomb form factors of 10B and 11B. *Nuclear Physics A*, **86**: 225-240.